Applied Mathematical Modelling 39 (2015) 1099–1118

Contents lists available at ScienceDirect

Applied Mathematical Modelling

journal homepage: www.elsevier.com/locate/apm

A nonlinear rotational, quasi-2DH, numerical model for spilling wave propagation

Antonino Viviano *, Rosaria E. Musumeci, Enrico Foti

Department of Civil and Environmental Engineering, University of Catania, viale Doria, 95125 Catania, Italy

ARTICLE INFO

Article history:
Received 21 February 2013
Received in revised form 17 June 2014
Accepted 22 July 2014
Available online 5 August 2014

Keywords:
Boussinesq
Breaking
Roller
Vorticity
Submerged shoal

ABSTRACT

The propagation of spilling waves interacting with complex bathymetries was studied by means of a new two-dimensional weakly dispersive, fully nonlinear Boussinesq-type of model. In particular, the governing equations were derived assuming the flow as rotational, and the effects of vorticity due to breaking were included through the surface roller concept, which was defined and implemented on the basis of a new algorithm developed for the purpose. The propagation of vorticity, due to wave breaking, is estimated under the assumption that the effect of convection is leading order with respect to the effect of vorticity-stretching and that the breaking phenomenon does not show high curvature on the horizontal plane. In particular, the dynamic problem is decoupled in a lateral direction considering a series of separated sections in which vorticity is solved. In this way it is possible to obtain rotational information along the domain to a reasonable computational cost. The numerical model was validated in a simple one-dimensional case and then applied to the study of breaking-generated vorticity due to wave motion over a submerged shoal.

1. Introduction

Boussinesq models are able to handle very efficiently several nearshore phenomena, such as refraction, diffraction, shoaling, reflection, combined wave-current flow and strong nonlinear interactions with rapidly varying bathymetry (see for example [1–9]). From the computational point of view, Boussinesq models are often solved by using finite difference methods on regular unstaggered or staggered numerical grids (see [2,10], respectively). This approach is usually preferred since it does not require an important programming effort. In order to deal with more realistic bathymetry, also in the presence of three-dimensional obstacles and multidirectional waves, finite element Boussinesq solvers have been successfully proposed [11–13].

However, when aiming at modeling the overall nearshore region, it must be stressed that the weakest point of such models is that they cannot deal with wave breaking. To face such a problem, several approaches have been introduced to include both a wave breaking criterion to trigger both the initiation and the end of a breaking event, and a breaking model able to describe the energy dissipation within the surf zone.

As regards the breaking onset criterion, two types of methodology were adopted, which rely (i) on the time derivative of the free surface elevation [14] or (ii) on the free surface slope [15]. As discussed in [16], it can be demonstrated that the two mentioned approaches are equivalent as regards to their effect on the momentum equation.

* Corresponding author. Tel.: +39 095 7382727; fax: +39 095 7382748.
E-mail addresses: nino.viviano@gmail.com (A. Viviano), rmusume@dica.unict.it (R.E. Musumeci), efoti@dica.unict.it (E. Foti).

http://dx.doi.org/10.1016/j.apm.2014.07.030
0307-904X/

Regarding the breaking model, two main strategies were adopted: (i) artificial eddy viscosity models [17,14] and (ii) surface roller models, which in turn can be subdivided into (a) non-explicit rotational models [15,18], and (b) rotational models [19–22].

Breaking models, based on the artificial breaking generated eddy viscosity, are simple from a computational point of view. Indeed, such an eddy viscosity is related to the time variation of free surface elevation. As demonstrated by Chen et al. [23], its application to the two-dimensional case is straightforward.

Concerning the surface roller approach, Svendsen [24] defined the roller as the 'volume of water carried by the wave with the wave celerity' on the front of a breaking wave. Breaking models based on such an approach try to mimic the dynamics of surf zone waves in a more realistic and physically based manner. For example, Schäffer et al. [15] applied the concept of the surface roller of a breaking wave in order to compute some additional terms in the momentum equation. The work was extended by Madsen et al. [18] to the two dimensional case. However, in the aforementioned models the implemented momentum equations seem to derive from the assumption of irrotational motion, i.e. starting from the Euler equation. Indeed, their additional breaking terms are related to the non-uniform simplified velocity profile rather than to the great amount of vorticity introduced by the breaking process.

Veeramony and Svendsen [19] included vorticity explicitly by deriving a weakly-nonlinear one-dimensional model starting from the Reynolds-averaged equations and by allowing horizontal vorticity to be introduced within the domain. In particular the source of vorticity is located along the lower edge of the surface roller; its value is determined by assuming the hydraulic similarity between breaking waves and hydraulic jumps. Musumeci et al. [22] extended such an approach by deriving a fully nonlinear version of the model, in order to obtain better shoaling properties close to the breaking point, and by implementing an original algorithm in order to avoid loss of vorticity.

In the present work, in order to deal with the rotational motion after breaking, a new set of 2D horizontal Boussinesq-type of equations have been derived which include the effects of vorticity, by extending the 1D fully nonlinear approach of Musumeci et al. [22], in order to develop a model able to deal with combined wave-current motion often forced by the presence of natural and artificial complex bathymetry conditions. An original numerical strategy has been developed with the aim of tracking the propagation of the surface roller over the horizontal plane.

The paper is organized as follows: in Section 2 the governing equations are derived along with the coupled vorticity transport equation; in Section 3 the numerical solution of the model is presented, with emphasis on the problem of tracking the rollers of breaking waves; in Section 4 the results of the model have been compared with experimental data from the literature for 1D and 2D nonbreaking and breaking waves; in Section 5 model results are analyzed in terms of vorticity dynamics. Finally in Section 6 the main conclusions of the work are drawn.

2. Schematization and formulation of the problem

Let us assume a cartesian coordinate system positioned in such a way that $\hat{x}$ and $\hat{y}$ are the horizontal coordinates, with $\hat{x}$ positive in the cross-shore direction, and $\hat{z}$ is the vertical one, equal to zero at the still water level. Fig. 1 shows the coordinate system along with the water depth $\hat{h}$ and the main variables of the problem, i.e. the three velocity components $\hat{u}$, $\hat{v}$ and $\hat{w}$ and the free surface elevation $\hat{\zeta}$. Hereinafter the symbol $\hat{}$ indicates dimensional quantities. The bottom is here assumed non erodible and impermeable. Moreover, the following dimensionless parameters have been chosen to be representative of the investigated flow: (i) the dispersive parameter $\mu = \hat{k}_0\hat{h}_0$ and (ii) the nonlinear parameter $\delta = \hat{a}_0/\hat{h}_0$, where $\hat{h}_0$ is the water depth at a reference location, and $\hat{k}_0$ and $\hat{a}_0$ are the corresponding wave number and wave amplitude respectively.

The independent variables can be appropriately made dimensionless as follows:

$$x = \hat{k}_0\hat{x}; \quad y = \hat{k}_0\hat{y}; \quad z = \frac{\hat{z}}{\hat{h}_0}; \quad t = \hat{k}_0\sqrt{g\hat{h}_0}\hat{t} \tag{1}$$

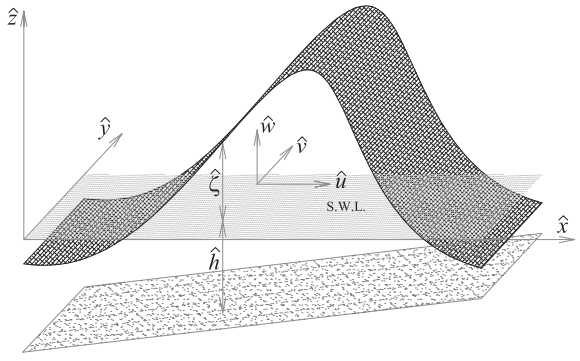

Fig. 1. Definition of the reference system and of the main variables (the velocity components $\hat{u}$, $\hat{v}$, $\hat{w}$ and the free surface elevation $\hat{\zeta}$) used in the present model.

while the free surface elevation, the pressure and the three velocity components in dimensionless form read:

$$\zeta = \frac{\hat{\zeta}}{\hat{a}_0}; \quad p = \frac{\hat{p}}{\rho g \hat{a}_0}, \tag{2}$$

$$u = \frac{\hat{u}}{\delta\sqrt{g\hat{h}_0}}; \quad v = \frac{\hat{v}}{\delta\sqrt{g\hat{h}_0}}; \quad w = \frac{\hat{w}}{\delta\mu\sqrt{g\hat{h}_0}}. \tag{3}$$

Since the flow after breaking is considered to be rotational in the present model, the vorticity field must also be solved. From the definition, the components of the vorticity are scaled as

$$\omega_x = \left(\mu^2\frac{\partial w}{\partial y} - \frac{\partial v}{\partial z}\right) = \frac{\hat{h}_0\hat{\omega}_x}{\delta\sqrt{g\hat{h}_0}}, \tag{4}$$

$$\omega_y = \left(\frac{\partial u}{\partial z} - \mu^2\frac{\partial w}{\partial x}\right) = \frac{\hat{h}_0\hat{\omega}_y}{\delta\sqrt{g\hat{h}_0}}, \tag{5}$$

$$\omega_z = \left(\frac{\partial v}{\partial x} - \frac{\partial u}{\partial y}\right) = \frac{\hat{h}_0\hat{\omega}_z}{\delta\mu\sqrt{g\hat{h}_0}}. \tag{6}$$

The goal of the present formulation is to obtain depth averaged equations. For such a reason the component ω_z will not be specified in the following but its effects are allowed in the proposed model. Moreover the two components of vorticity along the horizontal plane are assumed to be related to each other, as a function of the direction of wave propagation. Although such an assumption seems to be in contrast with the actual evolution of vorticity which is three-dimensional [25], it is acceptable near the front face of the breaking wave, i.e. where the greatest amount of dissipation appears [25].

In order to model the turbulent shear stresses, an eddy viscosity $\hat{\nu}_t$ is introduced, which in dimensionless term is

$$\nu_t = \frac{\hat{\nu}_t}{C_\nu\hat{h}_0\sqrt{g\hat{h}_0}}, \tag{7}$$

where ν_t is the dimensionless eddy viscosity and C_ν is a coefficient which can be empirically estimated to be about $0.01 \div 0.03$ [26].

The depth-averaged dimensionless continuity and Reynolds' equations read:

$$\frac{\partial\zeta}{\partial t} + \frac{\partial}{\partial x}\int_{-h}^{\delta\zeta} u dz + \frac{\partial}{\partial y}\int_{-h}^{\delta\zeta} v dz = 0, \tag{8}$$

$$\begin{aligned}\frac{\partial}{\partial t}\int_{-h}^{\delta\zeta}\mathbf{u}dz + \delta\left(\nabla\cdot\int_{-h}^{\delta\zeta}\mathbf{u}\right)\mathbf{u}dz + (\delta\zeta+h)\nabla\zeta - \mu^2\int_{-h}^{\delta\zeta}\frac{\partial}{\partial t}\nabla\int_z^{\delta\zeta}\left(\nabla\cdot\int_{-h}^{z}\mathbf{u}dz\right)dzdz - \delta\mu^2\int_{-h}^{\delta\zeta}\nabla\left(\nabla\cdot\int_{-h}^{z}\mathbf{u}dz\right)^2 dz \\ - \mu^2\int_{-h}^{\delta\zeta}\nabla\left(\nabla\cdot\int_z^{\delta\zeta}\nu_t\frac{\partial\mathbf{u}}{\partial z}dz\right)dz - \mu^2\nabla^\star\int_{-h}^{\delta\zeta}\nu_t(\nabla^\star\cdot\mathbf{u})dz - \delta\mu^2\int_{-h}^{\delta\zeta}\nabla\left[\nabla\cdot\int_z^{\delta\zeta}\mathbf{u}\left(\nabla\cdot\int_{-h}^{z}\mathbf{u}dz\right)dz\right]dz = O(\mu^4)\end{aligned} \tag{9}$$

with

$$\nabla = \left(\frac{\partial}{\partial x}, \frac{\partial}{\partial y}\right); \quad \nabla^\star = \left(\frac{\partial}{\partial y}, \frac{\partial}{\partial x}\right); \mathbf{u} = (u, v) \tag{10}$$

In order to derive the Boussinesq equations, a reference velocity must be introduced. Several choices are possible, as the depth-averaged velocity or the velocity at a specific elevation; an extensive discussion about the consequences of each choice is reported in Madsen and Schäffer [4]. In the present case the depth-averaged velocity, defined in vectorial dimensionless form as:

$$\bar{\mathbf{u}} = \frac{1}{h+\delta\zeta}\int_{-h}^{\delta\zeta}\mathbf{u}dz \tag{11}$$

has been considered, where $\bar{\mathbf{u}}$ is the horizontal velocity $(\bar{u}, \bar{v})$.

In order to feed Eqs. (8) and (9) with a velocity profile, the definition of vorticity will be taken as the starting point. Particularly from the vorticity components:

$$\omega_y = \frac{\partial u}{\partial z} - \mu^2\frac{\partial w}{\partial x}, \tag{12}$$

$$\omega_x = -\frac{\partial v}{\partial z} + \mu^2\frac{\partial w}{\partial y} \tag{13}$$

by integrating them along the water column, it is possible to obtain the two components of the vertical distribution of the vector $\mathbf{u}$, in terms of the bottom velocity $\mathbf{u}_b = (u_b, v_b) = \mathbf{u}(-h)$:

$$u(z) = u_b - \mu^2 \int_{-h}^{z} \frac{\partial^2}{\partial x^2}[u_b(h+z)]dz - \mu^2 \int_{-h}^{z} \frac{\partial^2}{\partial x \partial y}[v_b(h+z)]dz - \mu^2 \int_{-h}^{z} \frac{\partial^2}{\partial x^2} \int_{-h}^{z} \int_{-h}^{z} \omega_y dzdzdz + \mu^2 \int_{-h}^{z} \frac{\partial^2}{\partial x \partial y} \int_{-h}^{z} \int_{-h}^{z} \omega_x dzdzdz + \int_{-h}^{z} \omega_y dz + O(\mu^4), \tag{14}$$

$$v(z) = v_b - \mu^2 \int_{-h}^{z} \frac{\partial^2}{\partial x \partial y}[u_b(h+z)]dz - \mu^2 \int_{-h}^{z} \frac{\partial^2}{\partial y^2}[v_b(h+z)]dz - \mu^2 \int_{-h}^{z} \frac{\partial^2}{\partial x \partial y} \int_{-h}^{z} \int_{-h}^{z} \omega_y dzdzdz + \mu^2 \int_{-h}^{z} \frac{\partial^2}{\partial y^2} \int_{-h}^{z} \int_{-h}^{z} \omega_x dzdzdz - \int_{-h}^{z} \omega_x dz + O(\mu^4). \tag{15}$$

The first three terms on the right-hand side of the Eqs. (14) and (15) do not depend on the vorticity, thus representing the irrotational component of the horizontal velocity vector, referred to as $\mathbf{u_p} = (u_p, v_p)$, which, in terms of the depth averaged potential velocity $\bar{\mathbf{u}}_\mathbf{p}$, can be expressed as

$$\mathbf{u_p}(z) = \bar{\mathbf{u}}_\mathbf{p} + \mu^2 \left(\frac{\Delta_1}{2} - z\right) \nabla[\nabla \cdot (h\bar{\mathbf{u}}_\mathbf{p})] + \frac{\mu^2}{2} \left(\frac{\Delta_2}{3} - z^2\right) \nabla(\nabla \cdot \bar{\mathbf{u}}_\mathbf{p}) + O(\mu^4) \tag{16}$$

with $\Delta_1 = \delta\zeta - h$ and $\Delta_2 = \delta^2\zeta^2 - \delta\zeta h + h^2$.

The other three terms are due to the presence of the breaking generated vorticity, thus giving rise to a rotational component of the horizontal velocity which, in vectorial form, is:

$$\mathbf{u_r}(z) = \int_{-h}^{z} \boldsymbol{\omega}^* dz - \mu^2 \int_{-h}^{z} \int_{-h}^{z} \int_{-h}^{z} \nabla(\nabla \cdot \boldsymbol{\omega}^*) dzdzdz + O(\mu^4), \tag{17}$$

where $\boldsymbol{\omega}^* = (\omega_y, -\omega_x)$. It has been assumed that $|\nabla h| = O(\mu^2)$.

In other words, the horizontal velocity within the surf zone can be expressed as the sum of a potential and a rotational part:

$$\mathbf{u} = \mathbf{u_p} + \mathbf{u_r} \tag{18}$$

Such a formulation for the velocity profile has been obtained here in a more general and flexible form with respect to the procedure proposed by Musumeci et al. [22] for the one-dimensional case. Indeed, in that work the authors adopted the stream function approach which is strictly two-dimensional on the vertical plane and it cannot be extended to the present case. Here simply the definition of horizontal vorticity has been used to derive Eqs. (14) and (15).

By introducing Eq. (18) into Eqs. (8) and (9), it is possible to express the continuity and combined momentum equations as

$$\frac{\partial \zeta}{\partial t} + \nabla \cdot [(h + \delta\zeta)\bar{\mathbf{u}}] = 0 \tag{19}$$

$$\bar{\mathbf{u}}_t + \delta(\bar{\mathbf{u}} \cdot \nabla)\bar{\mathbf{u}} + \nabla\zeta + \mu^2 \left[\left(B - \frac{1}{3}\right) h^2 \nabla(\nabla \cdot \bar{\mathbf{u}}_t) - \frac{1}{2} h \nabla(\bar{\mathbf{u}}_t \cdot \nabla h) - \frac{1}{2} h(\nabla \cdot \bar{\mathbf{u}}_t)\nabla h + Bh^2 \nabla(\nabla \cdot \nabla\zeta)\right] + \delta\mu^2 \mathbf{K_1} + \delta^2\mu^2 \mathbf{K_2} + \delta^3\mu^2 \mathbf{K_3} + \{\delta\nabla(\boldsymbol{\Delta M}) + \delta\mu^2 \nabla(\boldsymbol{\Delta M_1}) + \mu^2[\nabla(\nabla \cdot \boldsymbol{\Delta P})]_t - \delta\mu^2 \mathbf{D_w} - \mu^2(\mathbf{D_{sv}} + \mathbf{D_{sh}}) - \delta\mu^2 \mathbf{D_{uw}}\}(h + \delta\zeta)^{-1} = 0 \tag{20}$$

where the subscript $(_t)$ indicates time derivatives and the three terms $\mathbf{K_1}$, $\mathbf{K_2}$ and $\mathbf{K_3}$ represent all the nonlinear components in which the vorticity is not present (see Appendix A for details). Moreover the well-known linear operator $\mathcal{L} = 1 + B\mu^2 h^2 \nabla^2$, proposed by Madsen and Schäffer [27] to improve the dispersion characteristics of the model in deeper water, has been used here.

It must be noticed that in Eq. (20) the dependency on the rotational velocity $\mathbf{u_r}$, which in turn is a function of the vorticity $\boldsymbol{\omega}^*$ injected inside the flow by the breaking mechanism, is included exclusively in the terms $\nabla(\boldsymbol{\Delta M})$, $\nabla(\boldsymbol{\Delta M_1})$, $[\nabla(\nabla \cdot \boldsymbol{\Delta P})]_t$, $\mathbf{D_w}$, $(\mathbf{D_{sv}} + \mathbf{D_{sh}})$ and $\mathbf{D_{uw}}$, which, in analogy to the work of Veeramony and Svendsen [19], are called *breaking terms*. They represent the excess of momentum flux due to breaking, which in turn is related to the dissipation of wave energy in the surf zone. In particular: $\mathbf{D_{sv}}$ and $\mathbf{D_{sh}}$ are the shear stresses inside the fluid which depend, respectively, on the turbulence along the vertical and the horizontal planes; $\nabla(\boldsymbol{\Delta M})$ and $(\nabla(\boldsymbol{\Delta M_1}))$ give the excess of momentum flux due to the vertical variation of the rotational velocity; $[\nabla(\nabla \cdot \boldsymbol{\Delta P})]_t$ is the contribution to the pressure due to the vertical motion; $\mathbf{D_w}$ is the excess of momentum due to the vertical motion and $\mathbf{D_{uw}}$ represents the interaction between the waves and the mean flow. The complete definition of the aforementioned terms is reported in the Appendix B.

For the one-dimensional flow case, such terms reduce to those found by Musumeci et al. [22]. In the two-dimensional case the exchange of momentum over the horizontal plane is much more complex, depending on the mutual nonlinear interaction between the two velocity components.

In the present model, the breaking terms in the momentum equation are functions of the vorticity field. In their classical paper Nadaoka et al. [25] analysed the turbulent structures under spilling breaking waves. In their Fig. 19, they show the presence of an high vorticity zone (maximum value of about 15 Hz) near the front face of the breaking wave, i.e. in the zone where the roller is usually defined. They found that the maximum of vorticity is one order of magnitude larger than in the

middle of the water column. It is specified that the corresponding vorticity structure has horizontal axis in the roller, it moves with the wave and its size is comparable with wave height. Watanabe et al. [28] have shown that undulations are present in the rear part of the primary vortex. Such undulations are created as evolution of the primary vortex by the vorticity stretching effect and they are amplified upstream leading to a vortex loop with counter-rotating vorticity. As a consequence of the mentioned works, it is possible to state that the lower point of the water column, i.e. approximately from the middle of the water column down to the bottom is mainly characterized by vorticity with vertical axis, i.e. ω_z. Such vorticity is one order of magnitude smaller than the vorticity along horizontal axis, which is dominant near the front face of the breaking waves. Therefore the relative errors introduced by neglecting ω_z can be estimated to be $O(0.1)$.

The bending of horizontal eddies has been studied also by Ting [29] for the solitary wave case by means of PIV measurements. The vorticity stretching effect is important for the generation of such oblique eddies in the rear part of the primary vortex. After that the vorticity becomes again convected by the flow induced by wave motion. Moreover Ting and Nelson [30] found that although the offshore transport of turbulence energy continued until the next breaker arrived, transport of turbulence energy perpendicular to the bed was confined to sporadic areas around impingement points after the growth phase. In view of the above experimental evidence, we take as acceptable to neglect the vertical vorticity with respect to the horizontal vorticity. Therefore in the proposed model it is assumed that within the surf zone the effect of convection is leading order with respect to the effect of vorticity stretching. Thanks to such an assumption, as a first approximation, the problem of determining the two-dimensional vorticity field can be reduced to a one-dimensional problem along the curvilinear abscissa s, defined in Fig. 2 as the direction of wave propagation.

From the results mentioned above, it follows that in order to compute the breaking terms the vorticity transport equation has to be solved as well. The boundary conditions of such a vorticity equation are available in the two-dimensional case along the vertical surfaces containing the wave rays, therefore the unknown variable ω is directed along a direction $\mathbf{n_s}$ normal to the curvilinear abscissa s corresponding to the generic wave ray. Turbulent diffusive-type processes across wave rays are neglected in the solution of the vorticity transport equation, however they are considered in the momentum equation. Therefore the vorticity along a wave ray may be indirectly influenced by the effects of vorticity on the nearby rays because the momentum equation takes into account vorticity-related turbulence diffusive effects, which vary in time. Moreover, as a consequence of the mild slope assumption generally adopted in Boussinesq-type models, the effects of vortex modification induced by the convergence or divergence of wave rays can be reasonably neglected, being smaller than local acceleration and convective terms. This argument can be demonstrated starting from the definition of longshore currents as a function of the radiation stresses. Indeed, the velocity component in the direction orthogonal to the wave ray, which is responsible of the vorticity stretching, should be proportional to the longshore current which in turn is proportional to the gradient of the water depth [31]. It is possible to analyse the order of magnitude of the convective and stretching terms of vorticity transport equation, starting from the scaling adopted in paragraph 2:

$$O\left(u_s \frac{\partial \omega_{ns}}{\partial s}\right) = O\left(\sqrt{gh}\frac{\sqrt{gh}}{h^2}\frac{\partial h}{\partial s}\right) = O\left(\frac{g}{h}\frac{\partial h}{\partial s}\right), \tag{21}$$

$$O\left(\omega_{ns} \frac{\partial u_n}{\partial n}\right) = O\left(\frac{\sqrt{gh}}{h}|\nabla h|\frac{\sqrt{gh}}{h}\frac{\partial h}{\partial n}\right) = O\left(\frac{g}{h}|\nabla h|\frac{\partial h}{\partial n}\right). \tag{22}$$

Since the term $|\nabla h| \ll 1$ because of the mild slope assumption, the stretching term in Eq. (22) is negligible with respect to the convective term (Eq. 21) when $\partial h/\partial n \leqslant \partial h/\partial s$. Let us consider now the angle θ between wave ray and the perpendicular to the isobath; the ratio between $\partial h/\partial n$ and $\partial h/\partial s$ is equal to $\tan\theta$. As a consequence the stretching term is negligible when $\theta \leqslant \pi/4$, i.e. when the bottom slope in n direction is less or equal to that along the s direction. Moreover the two terms in the vorticity equation are of the same order of magnitude only when $\tan\theta \gg 1$, i.e. when the direction of propagation is quasi-parallel to the bathymetry. Such a condition is rarely encountered also for waves propagating over complex bathymetries, when the bottom is mildly changing, therefore the stretching term of vorticity transport equation can be reasonably neglected.

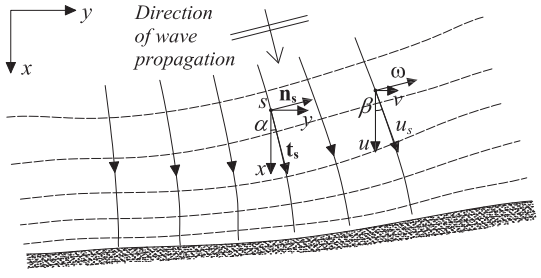

Fig. 2. Plan view of a wave ray field with indication of the curvilinear abscissa s and of the horizontal velocity u_s.

Under this assumption, the vorticity ω can be easily related to the vorticity vector defined by its components along the Cartesian abscissas, i.e. $\boldsymbol{\omega} = (\omega_x, \omega_y)$. To this aim, the components along the Cartesian abscissas of the unit vector respectively tangential and normal to the abscissa s can be obtained as equal to $(\cos\alpha, \sin\alpha)$ and $(-\sin\alpha,\ \cos\alpha)$, respectively, where α is the angle that the tangential direction $\mathbf{t_s}$ of the wave rays forms with the positive versus of the x. It follows that the vorticity along the tangential direction is assumed to be equal to zero. This means that the angle β, defined in Fig. 2 as the angle between the x axis and the direction of the velocity, is equal to the angle α. The relationship between $\boldsymbol{\omega}$ and its tangential and normal component (ω) in the direction of wave propagation can be then written as follows:

$$\omega_{ts} = \boldsymbol{\omega} \cdot \mathbf{t_s} = \omega_x \cos\alpha + \omega_y \sin\alpha = 0 \tag{23}$$

$$\omega_{ns} = \boldsymbol{\omega} \cdot \mathbf{n_s} = -\omega_x \sin\alpha + \omega_y \cos\alpha = \omega \tag{24}$$

The vorticity along $\mathbf{n_s}$ is the unknown variable of the following dimensionless vorticity transport equation along the abscissa s, which has been obtained by cross-differentiating the Reynolds-averaged Navier–Stokes equations and by applying the scaling arguments described above:

$$\frac{\partial\omega}{\partial t} + \delta u_s \frac{\partial\omega}{\partial s} + \delta w \frac{\partial\omega}{\partial z} = \nu_t \left(\mu^2 \frac{\partial^2\omega}{\partial s^2} + \frac{\partial^2\omega}{\partial z^2} \right), \tag{25}$$

where u_s is the dimensionless horizontal velocity in the direction of wave propagation, which has the modulus of the horizontal velocity $\mathbf{u}$. The eddy viscosity ν_t in Eq. (25) is here assumed to be constant. With reference to Fig. 3, the boundary and the initial conditions for the vorticity transport equation in dimensionless form are

$$\omega(s, z = \delta\zeta_e, t) = \omega_s, \tag{26}$$

$$\omega(s, z = -h, t) = 0, \tag{27}$$

$$\omega(s, z, t = 0) = 0 \tag{28}$$

in which ζ_e is the elevation of the lower edge of the roller and ω_s is the vorticity generated from the surface roller of the breaking wave. Therefore vorticity is "pumped" inside the water column from the highly turbulent region which is present on the top of the wave during the breaking phenomenon.

As regards the depth-dependency of ν_t, [21] investigated the effects of several eddy viscosity profiles numerically integrating Eq. (25). Their results show how the depth-constant eddy viscosity profile is able to reproduce velocity profiles under breaking waves as reasonably as other more complex choices. Moreover, if ν_t is constant along the water column, also an analytic solution of Eq. (25) can be found. Here the latter approach has been preferred since it is computationally more efficient. In particular, to obtain an analytical solution, the physical coordinates (s, z, t) are changed into the stretched computational coordinates (s, σ, t), where the new vertical coordinate σ is defined as

$$\sigma = \frac{h + z}{h + \delta\zeta_e} \tag{29}$$

so that the computational domain is changed from the time-dependent domain $-h \leqslant z \leqslant \delta\zeta_e$ to the rectangular time-constant domain $0 \leqslant \sigma \leqslant 1$. By perturbing the solution in terms of the small parameter δ the solution of the problems at $O(\delta)$ is

$$\omega = \sigma\omega_s + \sum_{n=1}^{\infty} \left[G_n^{(1)} + \delta G_n^{(2)} \right] \sin n\pi\sigma + O(\delta^2), \tag{30}$$

where the coefficients of the series $G_n^{(1)}$ are only function of x and t and the series $G_n^{(2)}$ represents the solution obtained considering terms $O(\delta)$. Therefore these two functions are defined as:

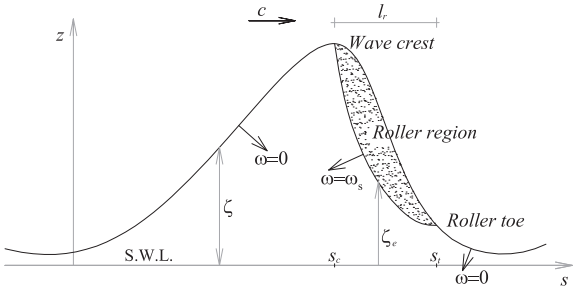

Fig. 3. Definition of a two-dimensional surface roller with indication of its geometry and of the points of injection of vorticity along the abscissa s, i.e. in the direction of wave propagation.

$$G_n^{(1)} = (-1)^n \frac{2}{n\pi} \int_0^t \frac{\partial \omega_s}{\partial t} e^{\kappa n^2 \pi^2 (\tau - t)} d\tau, \tag{31}$$

$$G_n^{(2)} = \int_0^t F_n^{(2)} e^{\kappa n^2 \pi^2 (\tau - t)} d\tau \tag{32}$$

in which:

$$\kappa = \frac{\nu_t}{h^2} \tag{33}$$

$$F_n^{(2)} = 2 \int_0^1 F^{(2)} \sin n\pi\sigma d\sigma \tag{34}$$

$$F^{(2)} = -2\kappa \frac{\zeta_e}{h} \frac{\partial^2 \omega^{(1)}}{\partial \sigma^2} + 2\omega_s \frac{\sigma}{h} \frac{\partial \zeta_e}{\partial t} + \frac{\sigma}{h} \frac{\partial \zeta_e}{\partial t} \frac{\partial \omega^{(1)}}{\partial \sigma} - u_s \frac{\partial \omega^{(1)}}{\partial s} - u_s \sigma \frac{\partial \omega_s}{\partial s} - \frac{w}{h} \left(\frac{\partial \omega^{(1)}}{\partial \sigma} + \omega_s \right). \tag{35}$$

For completeness sake in Appendix C the complete derivation of the breaking terms, obtained by substituting Eqs. (30)–(35) into the expressions (46)–(56) of Appendix B, is reported.

3. Numerical solution of wave breaking propagation

The numerical scheme chosen to integrate the momentum and the continuity equations is always a crucial point, indeed it can make the difference between an accurate and efficient model and a poor one. As far as extended Boussinesq models are concerned, a widely adopted numerical solution strategy is the one proposed by Wei et al. [2], who successfully applied a fifth-order finite difference scheme for the spatial derivatives and a third-order predictor, fourth-order corrector scheme for the integration in time, known in the literature as Adams–Bashforth–Moulton or ABM scheme. The same approach has been used here since it allows to take advantage both of the relatively fast explicit scheme and of the high accuracy of the spatial derivative discretization.

As regards the offshore and the lateral boundary conditions, the computational grid is constituted by a rectangle in which three of the boundaries, namely the lateral ones and the onshore one, are vertical walls and the other one is the offshore boundary. In particular, in such a first version of the model the attention has been concentrated only on the breaking related phenomena, therefore no run-up condition has been considered. The condition at the vertical walls is that the horizontal velocity component is zero, which is an artificial condition for many applications. In order to overcome such a problem a sponge layer can be inserted in front of each of the walls. At the offshore boundary an absorbing-generating boundary condition is applied, similar to that proposed by Vandongeren and Svendsen [32] in their nonlinear shallow water equation model; however in the present case the forcing term includes also the dispersive effects which are taken into account in Boussinesq models.

Concerning the breaking generated vorticity in 2DH case, even along the same wave front the roller can show different characteristics or it may not even be present at all at some locations. In order to demonstrate how each spatial point is characterized by different conditions of wave breaking, in Fig. 4 an image of a curvilinear wave front within the surf zone is shown.

To cope with such a problem, the proposed approach is to consider the so called "3D roller" as composed of several two-dimensional rollers which are placed on the vertical surfaces which follow the direction of wave propagation. By adopting such a simple schematization, the generic roller is always located along the above defined curvilinear abscissa s, and a breaking wave can be discretized along a series of wave rays always tangential to the horizontal velocity, as shown in Fig. 2. The original three-dimensional problem is then reduced to a series of separated two-dimensional problems solved along sections which do not directly pass each other information on the vorticity evolution in the lateral direction, unless through turbulent diffusion. The two-dimensional roller along each curvilinear axis can be used to specify the vorticity boundary conditions, necessary for the analytical solution of the vorticity transport equation.

In analogy to the work of Veeramony and Svendsen [19], the hydraulic similarity between breaking waves and hydraulic jumps has been used here to specify the geometry of the surface roller and the value of ω_s along the lower edge of the roller, whose elevation is ζ_e. In particular such a task has been accomplished by using two functions obtained as best fit of the experimental data obtained for low Froude number hydraulic jumps by Svendsen et al. [33]:

$$\frac{\omega_s h_2 \xi}{U_1} = 15.75 \left(1 - \frac{x'}{l_r} \right), \tag{36}$$

$$\zeta_e = \zeta - 0.78 h_2 \sqrt{\xi} e^{-\frac{x'}{l_r}} \left(\frac{x'}{l_r} - \frac{x'^2}{l_r^2} \right), \tag{37}$$

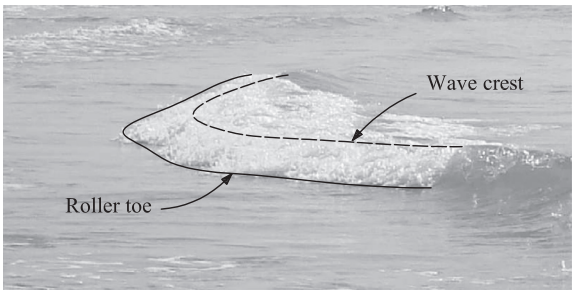

Fig. 4. Image of a curvilinear wave front within the surf zone where each spatial point is characterized by different condition of wave breaking.

where ξ is the ratio h_2/h_1, h_1 and h_2 represent the minimum water depth before the jump and the undisturbed water depth downstream with respect to the jump, respectively, U_1 is a supercritical reference velocity, and x' is the horizontal coordinate, which for breaking waves is equivalent to a reference system moving at the wave speed.

A critical point, which is common to all the Boussinesq-type of models, is to establish a criterion for the onset of breaking, which is here complicated by the need to determine also the location of the 3D roller. In the proposed model it is assumed to trigger breaking when and where the local steepness of the wave front exceeds a critical surface gradient, equal to $\tan\phi$. Precisely, the toe of the roller is defined as the location where the wave steepness is identical to $\tan\phi$ and the roller itself is included between its toe and the wave crest. In order to account for the transition from the initial breaker to the bore-like stage within the inner surf zone, the critical roller angle, ϕ, is assumed to decrease from ϕ_B up to its final value ϕ_0 as a function of the age τ of the roller. The relation used here, initially introduced by Schäffer and Madsen [15], is

$$\tan\phi = \tan\phi_0 + (\tan\phi_B - \tan\phi_0)\exp\left\{-\ln\left[2\left(\frac{\tau - t_B}{t_{1/2}}\right)\right]\right\} \tag{38}$$

in which τ represents the time interval measured from the initiation of wave breaking, $t_{1/2}$ defines the time scale for the development of the roller, and t_B is the time of incipient breaking. Such a criterion permits a reliable definition of the toe position, where the injection of vorticity is strongest.

In two horizontal dimensions, as shown in Fig. 5, the toe of the roller becomes a curve which can be defined as the points satisfying the condition that the absolute value of the surface elevation gradient $|\nabla\zeta|$ equals the instantaneous local value of $\tan\phi$ and that the gradient in the direction of the wave propagation is negative.

Even though the surface roller detection appears quite simple to be determined in a continuous description, such a detection becomes rather complex over a numerical grid, where a discrete representation of the spatial variation of the hydrodynamic variables along the roller is required.

In the past Sørensen et al. [34] faced such a problem by using a staggered grid for the determination of the toe points, by assuming a linear variation between two toe points and by defining the roller as the area comprised between each couple of toe points and the projection on the horizontal plane of the two lines tangential to the direction of wave propagation.

Another approach has been introduced more recently by Sørensen et al. [35] which bases the individuation of the toe of the roller on the time derivative of the free surface elevation. The corresponding algorithm is simple in 2DH, as it is in 1DH, but it does not provide the roller geometry which is needed in our model to use the hydraulic jump similarity. Therefore we adopt a new approach in our work which is similar to that of Sørensen et al. [34] and which is described below.

With reference to Fig. 6, it must be preliminarily stressed that the Boussinesq equations are derived over a rectangular grid; therefore the dependent variables ζ and $\mathbf{u}$ are known at each grid point. Instead, the surface elevation gradient, i.e. the vector $(\partial\zeta/\partial y,\ \partial\zeta/\partial x)$, and the direction of wave propagation α, defined as

$$\tan\alpha = \frac{\partial\zeta/\partial y}{\partial\zeta/\partial x} \tag{39}$$

are calculated in the correspondence of the central nodes of the rectangular grid (i.e. at the circles in Fig. 6). Thus according to the breaking criterion, the toe location is found along the light-dashed lines in Fig. 6, by means of a linear interpolation, where both the following conditions are satisfied

$$\frac{\partial\zeta}{\partial s} < 0, \tag{40}$$

$$\tan\alpha = |\nabla\zeta|. \tag{41}$$

In order to get the complete roller geometry, the wave crest must also be located. Such a task is achieved here by determining the maximum of the surface elevation at the staggered grid for each wave, so that the wave crest curve is defined. Therefore the roller in the direction of wave propagation, i.e. along the curvilinear abscissa s, is determined and the vorticity transport equation can be solved.

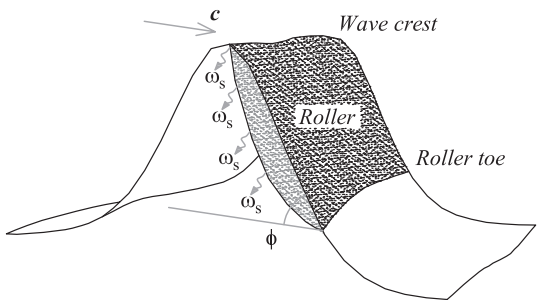

Fig. 5. Sketch of a three-dimensional roller with injection of the vorticity ω_s at its lower boundary; c is the wave celerity, ϕ is the angle at the toe of the roller which influences the breaking onset criterion.

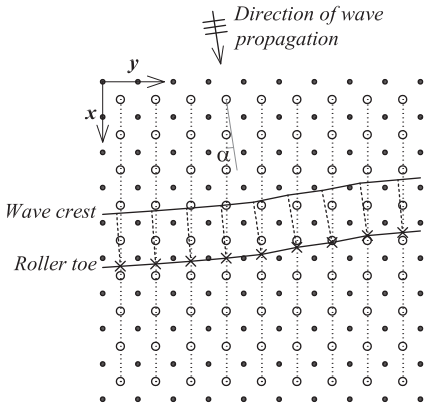

Fig. 6. Top view of the numerical grid in which the roller toe points (×), rectangular grid (•) and staggered grid (○) nodes are showed, the broken lines represent the sections in which injection of vorticity is computed.

In summary, the computations of vorticity and breaking terms are executed directly on the fixed grid used for the solution of Boussinesq equation, so the wave ray pattern is here adopted only for the definition of the roller, from which the injection of vorticity ω_s can be estimated. As a consequence the wave rays are detected only in the region where the roller is defined: between its toe and the wave crest. In such a context the example of computed ray pattern in Fig. 7 represents the roller sub-grids, obtained from the 3D roller tracking algorithm on the basis of the free surface distribution. In the following the steps used by such an algorithm are summarized: (i) the free surface gradient is computed at the middle points between fixed nodes; (ii) the toe of the roller is obtained as the point at which the surface gradient equals the tangent of the critical roller angle; (iii) each roller sub-grid is straight and it ends backwards at the wave crest; (iv) the injection of vorticity is computed along the roller sub-grids and interpolated onto the fixed grid, at which vorticity and breaking terms can be obtained and thus added to the momentum equation within the surf zone. A fairly important consequence of the proposed procedure is that the interpolation of the variable between ray pattern and fixed grid bypasses problems related to ray crossing, which may take place for wave propagating over a complex bathymetry.

More in details, the lower edge of the roller ζ_e and the injection of vorticity ω_s are computed along the sections passing through the toe points (broken lines in Fig. 6 or blue lines in Fig. 7), by applying expressions (36) and (37). Finally the age of the roller is updated and the corresponding toe angle ϕ can be calculated according to Eq. (38). Once the toe curves of the rollers, which are present in the domain, have been obtained at a generic time step n, their position, age and distribution of ω_s are stored; in such a way these values are ready to be used at the next time step, $n+1$, for the calculation of the term $\partial\omega_s/\partial t$, which is necessary for the analytical solution of the vorticity transport equation and of the breaking terms.

It follows that due to such a complex definition of the roller position in the proposed 2DH model, the vorticity and the breaking terms of the momentum equations are computed here directly on the fixed grid, i.e. where the Boussinesq equations are solved. Such an approach represents a simplification of the 1DH solution scheme used by Musumeci et al. [22], in which the vorticity is solved along the so called "moving subgrid" and where a more detailed description of the breaking related loss of energy is carried out.

The activation of the algorithm discussed above is performed when the waves start to break. Two tests have been carried out, with the same conditions but slightly different wave height, in order to estimate the increase of computational time due to the wave breaking module. The CPU used is an "Intel Pentium D" having frequency of 3.00 GHz and cache memory equals to 2 MB. The resulting increase of estimated computational time is 147%. As for the memory cost, it is equal to 1.86 GB for all

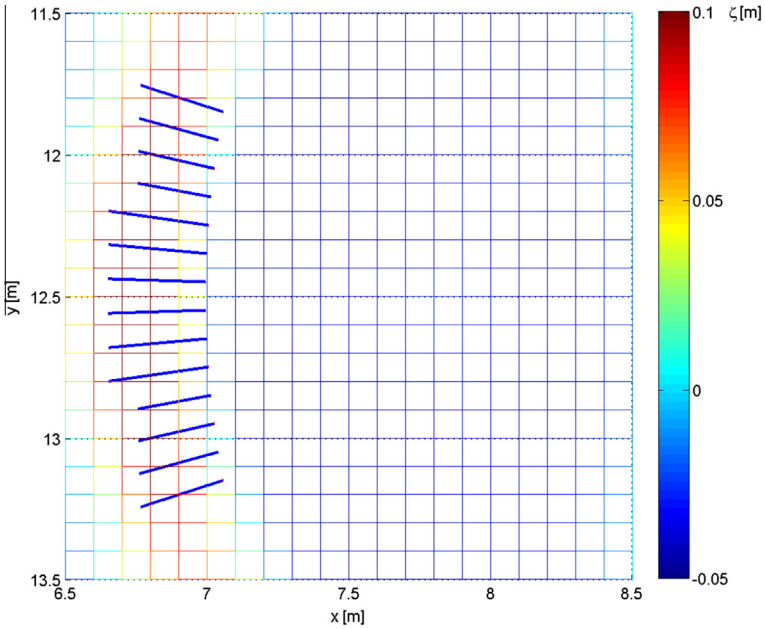

Fig. 7. Plan view of an example of ray pattern at which injection of vorticity is computed, obtained from the computed free surface elevation.

the wave conditions, since the variables are defined in a static fashion and thus the space of memory is allocated only once at the beginning of the run.

4. Validation of the model

The main characteristic of the proposed model is its capability of simulating the breaking generated vorticity and, in turn, of taking into account the energy dissipation. Before applying the proposed model in 2DH conditions, its behavior at breaking has been investigated by simulating the 1D case of periodic waves propagating in a straight channel over a constant slope. In particular, the experimental data of Hansen and Svendsen [36] on the breaking of cnoidal waves has been used as a benchmark. Such experiments have been conducted in a wave flume which is: 32 m long and 0.6 m wide; the steepness of the sloping part was 1:34.26. The corresponding numerical tank, sketched in Fig. 8, is shorter than the actual one because an initial flat bottom greater than one wave length is not necessary for the incident wave stabilization. The waves generated at the offshore boundary are cnoidal waves, with wave height $H = 0.04$ m and period $T = 2.5$ s, the critical value of wave slope at which the waves are considered to break is $\phi_B = 30^\circ$.

The model results are compared with experimental data in Fig. 9(a), while the same comparison obtained by means of the 1D Boussinesq model of Musumeci et al. [22] is shown as a reference (Fig. 9(b)). In particular the free surface elevation has been plotted every 0.074 s, that is the time interval covering ten computational time steps.

In the shoaling region, both models show a very similar behavior. From the off-shore boundary (at $x = 0$) up to $x \simeq 10$ m, it is recognizable a gradual increase of the wave crests level, which corresponds to an increase of wave height. In both models such a behavior overlaps the experimental results of [36], which are expressed by the black diamonds in the same Fig. 9. Some differences are present at through level (starting from $x = 8$ m). In particular, the proposed model results show oscillations of the lower free surface envelope having amplitude equal to that of the 1D model (2 mm) and length smaller of about 4 times with respect to the 1D model results. Such oscillations are due to numerical instabilities generated in the breaking zone and propagated back in the shoaling region.

As for the model results within the surf zone, the comparisons deserve some more comments. First of all, the wave height in the area of initiation of the breaking phenomenon is slightly underpredicted from both the analyzed models. In particular, the proposed two dimensional model predicts a maximum level of the wave crest which is 5% lower than the corresponding one obtained by the one-dimensional model. This difference is a consequence of the different numerical strategy used to detect the breaking point in the two models. Indeed, in the proposed model the values of the gradient are calculated on the staggered grid, so causing a spatial averaging of variables, whereas in Musumeci et al. [22] a polynomial interpolation was adopted. In the inner surf zone the results show other differences. In fact the proposed model maintains higher wave heights in comparison to the one-dimensional model, even though the results are still in a fairly good agreement with the experimental data. This behavior can be explained by considering the differences in the definition of the subgrid, over

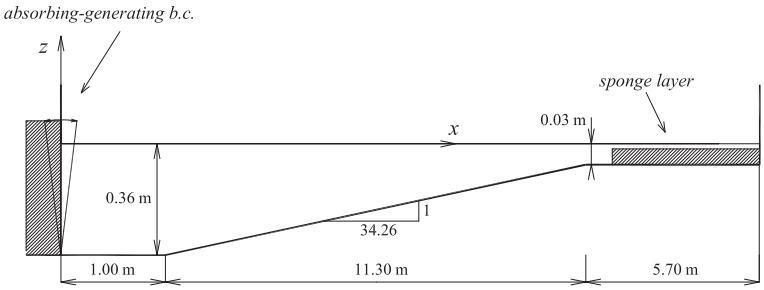

Fig. 8. Sketch of the numerical wave tank used to simulate the experimental set-up of Hansen and Svendsen [36]. In the y direction the flume is 1 m wide.

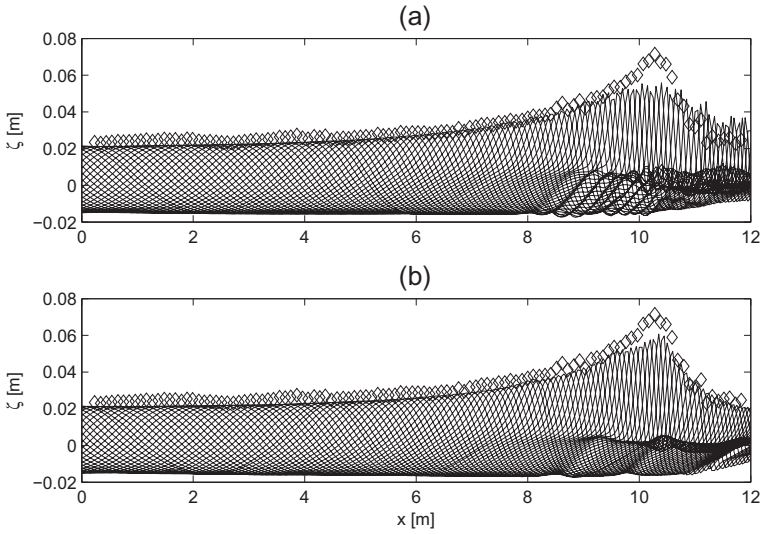

Fig. 9. Free surface elevation registered every 0.074 s. The diamonds represent the maximum surface elevation obtained by Hansen and Svendsen [36]. Numerical results of the: (a) proposed two-dimensional model; (b) model by Musumeci et al. [22].

which breaking terms related to vorticity are computed (see Section 3 for details). Nevertheless, the results of the proposed two-dimensional model are still in agreement both with its parent one-dimensional version and with the experimental data.

In order to compare the velocity field induced by turbulent motion under spilling breakers, another validation has been carried out considering the laboratory study of Huang et al. [37]. Such a study considers incident monochromatic waves with 1.0 s wave period and 3.0 cm wave height. The waves are generated at the constant water depth of 35.9 cm. The slope of the bottom is uniform and it is equal to 1/20. The instantaneous velocity field was measured within the surf zone by using Particle Image Velocimetry (PIV). Due to the large extension of the region interested by the breaking phenomenon, seven PIV fields of view were mosaicked to form a continuous flow field. The velocity fields measured within the surf zone by Huang et al. [37] are shown in Fig. 10.

The incident waves and the numerical domain used for the present validation have the same characteristics of the laboratory setup described above, with the exception of the swash zone which has been substituted with a numerical absorbing sponge layer, having water depth equal to 5 mm. The spatial discretization is obtained by considering $dx = 5$ cm and the integration in time by using dt equal to 0.01 s.

The obtained results are showed in Fig. 11 in terms of velocity field at 5 instants covering the whole wave period. The results are plotted in such a way to allow a direct comparison with the available experimental data [37].

In particular, the calculated velocity field shows that the solution of the proposed model is in a fairly good accordance with the laboratory results up to $t/T = 0.3$. Indeed looking at the plots (a) and (b) of Fig. 11, it can be noticed that the velocity is directed upward under the roller and its intensity increases near the lower edge of the roller, reaching values greater than 0.5 m/s as in the experiments. In this case, the relative errors on the maximum velocity is estimated to be less than 10%. At the following stages of breaking, the maximum measured velocities of about 0.3 m/s are confined near the roller, where the present model gives values less than 0.2 m/s. Such a discrepancy is probably due to the fact that the present model is not able to simulates the variation of vorticity direction, which occurs in the inner surf zone.

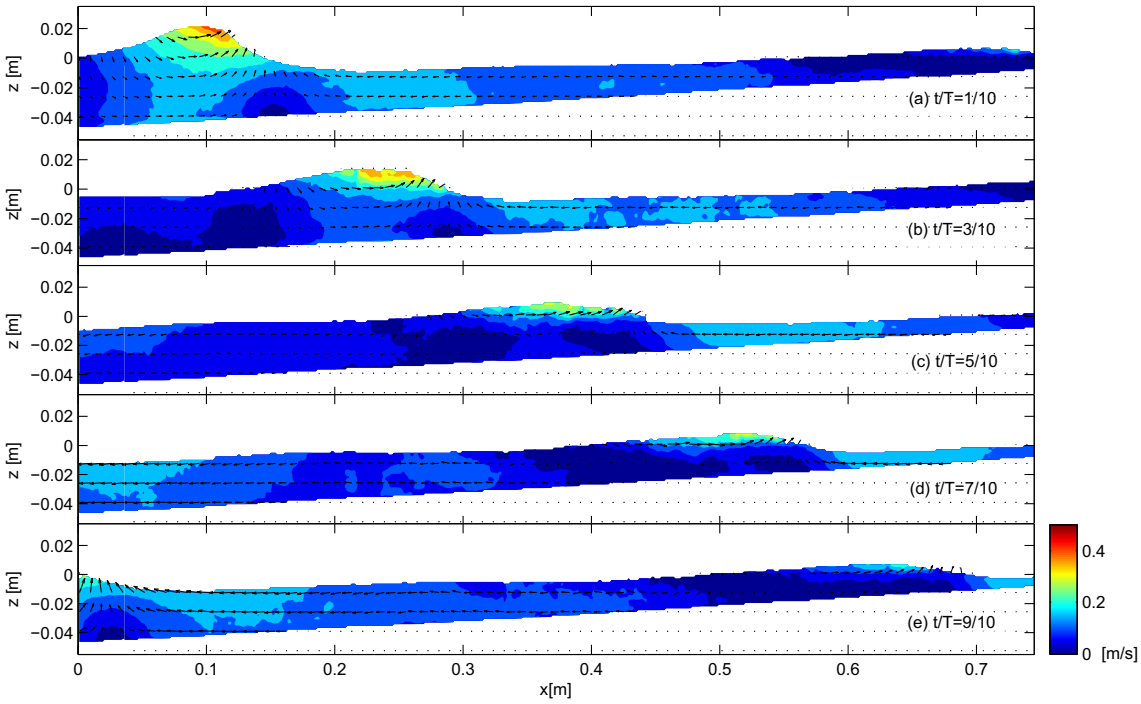

Fig. 10. Measured velocity fields in the surf zone at 5 time steps covering a whole wave period, from the experiments of Huang et al. [37].

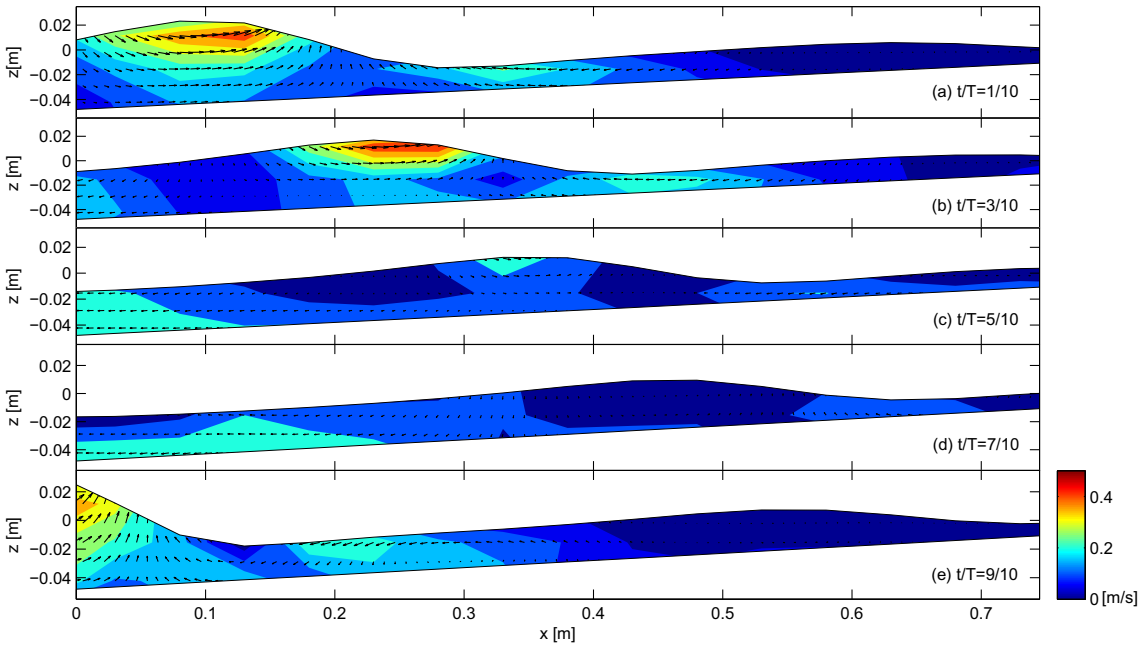

Fig. 11. Computed velocity fields in the surf zone at 5 time steps covering a whole wave period for the experimental conditions of Huang et al. [37].

5. Vorticity dynamics

The innovative characteristic of the present model is the possibility to consider the presence of breaking induced vorticity inside the flow domain. In order to qualitatively validate the proposed model capabilities in estimating vorticity, the model of Dimakopoulos and Dimas [38] has been taken into account. Such authors developed a large-wave simulation method (LWS) coupled with a subgrid scale model (SGS) for turbulence, to obtain the vorticity induced by oblique spilling breaking waves propagating over a plane bottom. They observed that the two components of horizontal vorticity have maximum values of 10.6 Hz and 3.6 Hz along x and y respectively. The magnitude of such horizontal vorticity is comparable to that

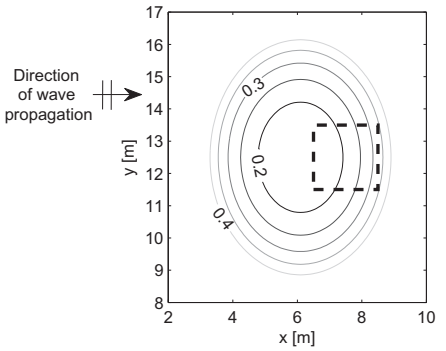

Fig. 12. Plan view of the shoal defined by Vincent and Briggs [39] with the location of the squared region in which the vorticity dynamics has been studied.

observed in the 1DH version of the model, as it was shown by Briganti et al. [21] in Fig. 7. Moreover Dimakopoulos and Dimas [38] considered the average ratio of these components in the roller area and they obtained that the direction of the resulting horizontal vorticity is almost perpendicular to the direction of wave propagation. Such a result confirms our assumption, introduced in Eq. (23) of Section 2, that $\omega_{ts} = 0$. As for the vertical vorticity the same authors showed that it is insignificant compared to the other two components and its magnitude does not exceed the value of 0.5 Hz which is consistent with our hypothesis of neglecting ω_z.

The above comparison allows us to analyse the vorticity behavior in a more complex case, i.e. the submerged shoal studied by Vincent and Briggs [39]. In such a case the direction of wave propagation is deviated by refraction caused by the shoal, which also determines an increase of wave steepness up to breaking.

In order to carry out a detailed analysis, the attention has been focused on a square region located onshore of the crest of the shoal (see Fig. 12). In Fig. 13 the contour plots of the spatial distribution of vorticity ω at the still water level (i.e. at $z = 0$)

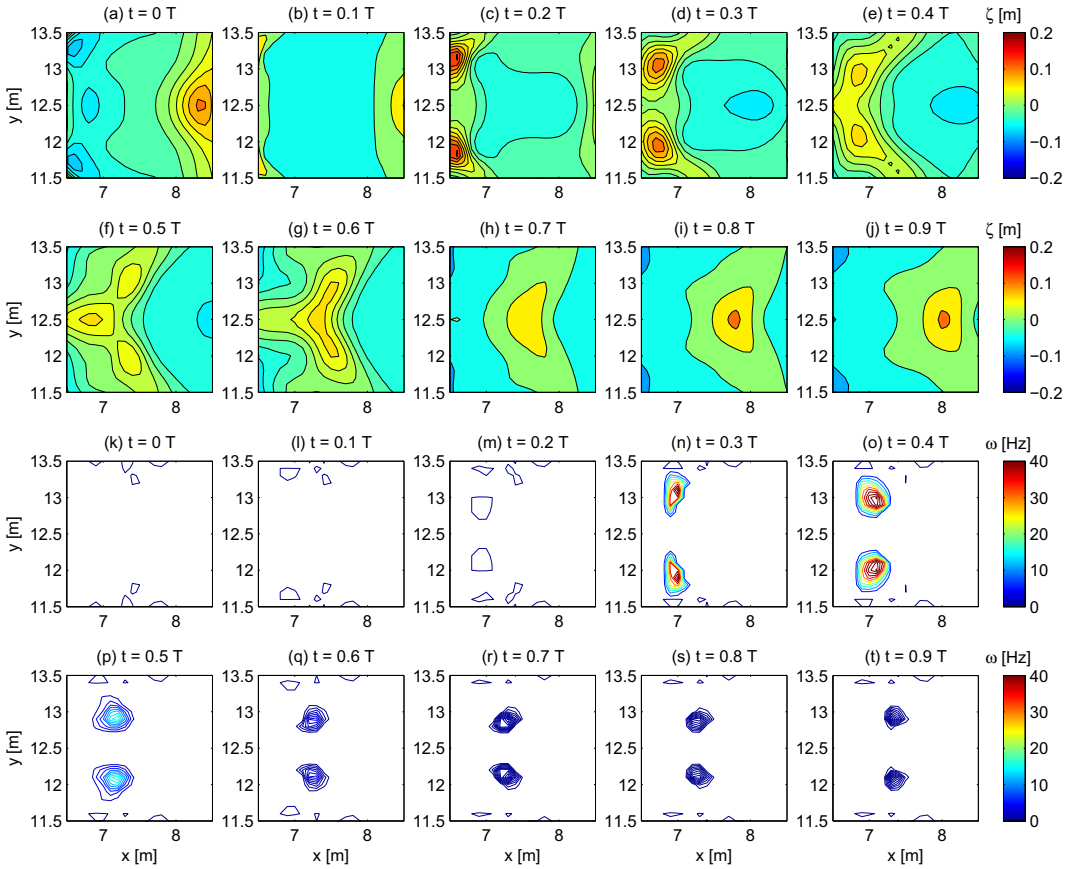

Fig. 13. Free surface elevations (a)–(j) and vorticity at $z = 0$ (k)–(t) at ten instants within a wave period.

within a wave period T are shown along with the corresponding contour plots of the surface elevations. In particular, Fig. 13(c) shows at its off-shore boundary a larger surface elevation gradient, which indicates the condition of incipient breaking at $t = 0.2T$; at the same time the corresponding vorticity distribution (Fig. 13(m)) provides negligible values. At the following instants (from $0.3T$ up to $0.5T$) the waves are still breaking, as demonstrated by the decreased elevation of the wave crest, while the vorticity increases suddenly, exceeding the value of 40 Hz. During the second half of the wave period, the slope of the free surface elevation is not large enough to maintain wave breaking, which stops. As a consequence, vorticity at $z = 0$ decreases both in intensity and in space.

Vorticity is present at the wave front at the initial instants of breaking (see for example Fig. 13(n) at $t = 0.3T$). During the following time steps, up to $t = 0.4T$, the planar extension of vorticity increases in both directions, extending also in the region offshore the wave crest. From such results it is clear that the proposed model is able to simulates the wake generated on the rear side of surf zone waves. Such a feature has been analyzed in the one dimensional case by Briganti et al. [21], who investigated the effects of a depth variant eddy viscosity, by solving numerically the vorticity transport equation in the model of Musumeci et al. [22]. In particular such authors obtained that, once the breaking is fully developed, a great amount of vorticity is present near the toe of the roller, which gradually decreases downward in the wake region.

The distribution of vorticity along the water column can be analyzed from Fig. 14, which shows the development of breaking generated vorticity at three elevations along the water column ($z = 0, -0.08$ and -0.16 m) during half wave period, starting from the breaking onset. In particular it is possible to observe that the greatest values of vorticity is present at the highest surface elevation, as expected. Moreover, the maximum value of vorticity is delayed going toward the bottom. Indeed for $z = -0.08$ m such a maximum is reached at the instant $0.4T$, i.e. after 1/5 of the wave period from the breaking initiation. Moving near the bottom (for $z = -0.16$ m) the maximum of vorticity has a low value of about 5 Hz and it is reached after $2/5T$ from the starting time steps of the breaking phenomenon.

The previous results can be qualitatively compared, for example, with the experimental results obtained by Nadaoka et al. [25]. They investigated the structure of turbulence by means of flow visualization techniques and of a fibre-optic LDV system. In their analyses, 'horizontal eddies' near the front of breaking waves and 'obliquely descending eddies' beside them, in the wake region are shown. As it has been demonstrated, the first horizontal axis vortical structure can be simulated by the proposed model because it is directly related to the vorticity injection within the roller region, which has an initial horizontal

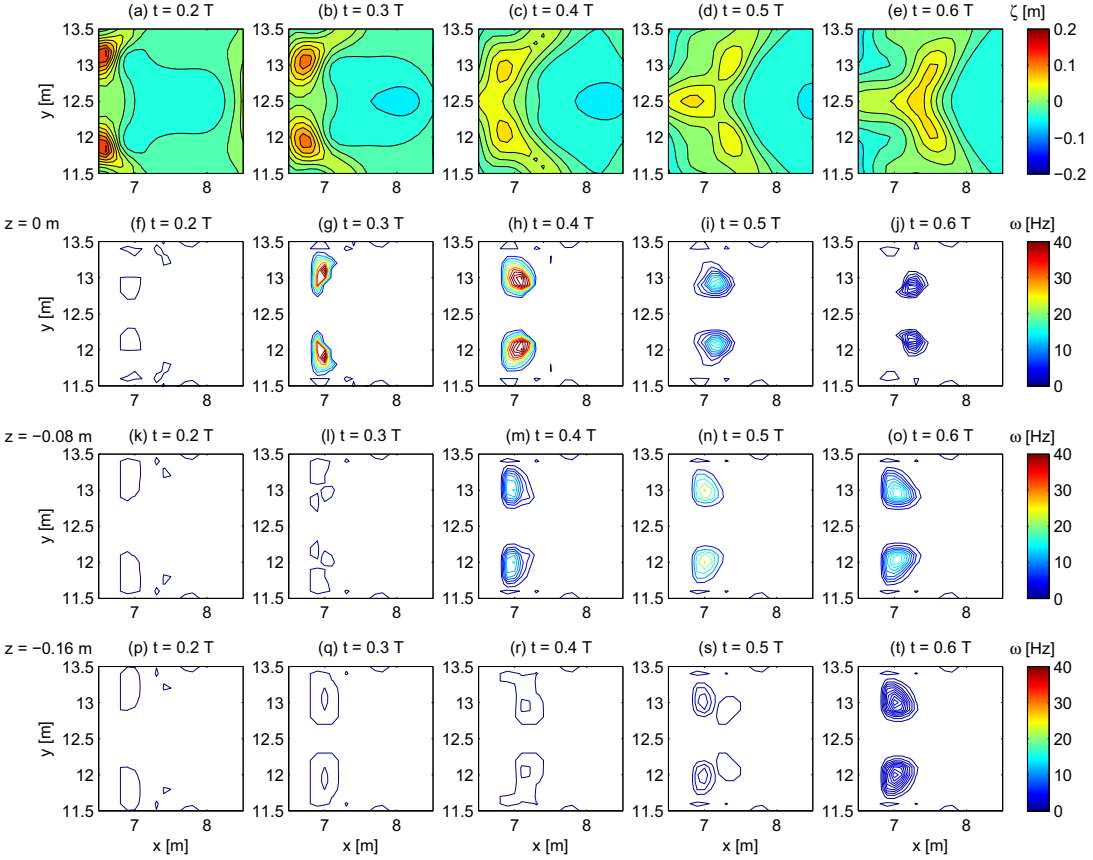

Fig. 14. Free surface elevations (a)–(e) and vorticity at $z = 0$ (f)–(j), $z = -0.08$ m (k)–(o) and $z = -0.16$ m (p)–(t) at five time steps covering half wave period.

axis. Instead, the subsequent obliquely turbulent structure cannot be caught by the present model because in such a region the vorticity is not acting on planes perpendicular to horizontal directions.

From a visual comparison between such experimental data and the vorticity distribution in the 1DH version of the proposed model, (see Fig. 19 of [22]) it is possible to observe that such a numerical model underestimates the vorticity under the wave trough. Indeed in Fig. 19 of Nadaoka et al. [25] a maximum value of vorticity of about 7 Hz is present under the trough of the wave. On the contrary in the same region the proposed model gives vorticity which is close to zero. Since, Nadaoka et al. [25] found that the greatest values of vorticity are present in the correspondence of horizontal eddies, it can be stated that the present model is at least able to capture the leading order vortical motion under breaking waves.

6. Concluding remarks

A new two-dimensional Boussinesq type of model was derived and implemented. The model is aimed to the study of flow driven by breaking waves in the surf zone, and in the presence of complex bathymetries.

The foremost characteristic of the proposed model is the presence of dissipating terms in the momentum equation, due to wave breaking. Such terms are not artificially imposed, but were derived from the assumption of rotational flow. In particular, the injection of vorticity inside the domain takes place from the free water surface and is only related to the presence of the roller. It is important to specify that the original three-dimensional problem of obtaining the vorticity distribution inside the domain was decoupled along the lateral direction by considering a series of separate two-dimensional problems. In this way the wave breaking evolution is modeled in a physically based manner, by simulating what actually happens during the propagation of spilling breakers.

The validation of the model was performed considering the one-dimensional case of periodic waves propagating orthogonally to the coastline over a sloping straight beach. This case was thoroughly analyzed in the previous literature by means of both numerical and physical models, therefore, several results are available for comparison. In the present contribution the experiments on cnoidal breaking waves of Hansen and Svendsen [36] (see Fig. 8) were used as a benchmark. Furthermore, the same data set was considered to validate the previous one-dimensional version of the present model (i.e. [19,22]). The analysis, (see Fig. 9) shows acceptable agreement in the shoaling region, 2 m before the breaking zone. Whereas, in the outer surf zone, the wave height is under-predicted by approximately 5% with respect to the one-dimensional model of Musumeci et al. [22]. Such instabilities are due to the high steepness of the waves, causing oscillations of the wave crest. As a result, it is more difficult to follow the actual shape of the breaking waves by the proposed 2D roller tracking algorithm.

Concerning the two-dimensional applications of the proposed model, the vorticity dynamics under breaking waves were investigated for the shoal case of Vincent and Briggs [39]. In particular, the attention was focused on a squared area located onshore with respect to the top of the shoal where wave breaking develops. The analysis on the space–time evolution of the computed vorticity shows that: (i) the vorticity increases rapidly in a small region near the roller and immediately below the free surface; (ii) the horizontal extension of the vorticity structure increases, thus, simulating the wake effect in the rear part of the wave crest (iii) this structure expands slowly along the water column, resulting in a delay effect of $2/5T$ between the initiation of the breaking phenomenon and the instant at which the maximum of vorticity is reached close to the bottom.

The above results show that, notwithstanding the limits and the simplifications of the present model, it represents a suitable step towards a better physically-based description of spilling wave breaking in Boussinesq-type of models.

Acknowledgement

This work has been partly supported by the research contract funded by the PRIN 2010–2011 project HYDROCAR, by the EC funded project HYDRALAB IV (contract No. 261520), and by the PON 2007–2013 project SEAPORT funded by MIUR (Italy).

Appendix A. Nonlinear terms

The vector variables $\mathbf{K_1}$, $\mathbf{K_2}$ and $\mathbf{K_3}$ correspond to the non linear terms in the combined momentum equation (20). They read as:

$$\begin{aligned}\mathbf{K_1} &= -\frac{1}{3}h^2\nabla[\bar{\mathbf{u}}\cdot\nabla(\nabla\cdot\bar{\mathbf{u}})] + \frac{2}{3}h^2(\nabla\cdot\bar{\mathbf{u}})\nabla(\nabla\cdot\bar{\mathbf{u}}) - \frac{1}{2}h\nabla[\bar{\mathbf{u}}\cdot\nabla(\bar{\mathbf{u}}\cdot\nabla h)] - \frac{1}{2}h[\bar{\mathbf{u}}\cdot\nabla(\nabla\cdot\bar{\mathbf{u}})]\nabla h \\ &+ \frac{1}{2}h(\nabla\cdot\bar{\mathbf{u}})^2\nabla h - h(\nabla\cdot\bar{\mathbf{u}}_t)\nabla\zeta - \frac{2}{3}h\zeta\nabla(\nabla\cdot\bar{\mathbf{u}}_t) - \frac{1}{2}\zeta(\nabla\cdot\bar{\mathbf{u}}_t)\nabla h - \frac{1}{2}\zeta\nabla(\bar{\mathbf{u}}_t\cdot\nabla h) - (\bar{\mathbf{u}}_t\cdot\nabla h)\nabla\zeta \\ &+ Bh^2\nabla[\nabla\cdot((\bar{\mathbf{u}}\cdot\nabla)\bar{\mathbf{u}})],\end{aligned} \tag{42}$$

$$\begin{aligned}\mathbf{K_2} &= -\frac{1}{3}\zeta^2\nabla(\nabla\cdot\bar{\mathbf{u}}_t) - \zeta(\nabla\cdot\bar{\mathbf{u}}_t)\nabla\zeta + \frac{4}{3}h\zeta(\nabla\cdot\bar{\mathbf{u}})\nabla(\nabla\cdot\bar{\mathbf{u}}) - \frac{2}{3}h\zeta\nabla[\bar{\mathbf{u}}\cdot\nabla(\nabla\cdot\bar{\mathbf{u}})] + h(\nabla\cdot\bar{\mathbf{u}})^2\nabla\zeta - h[\bar{\mathbf{u}}\cdot\nabla(\nabla\cdot\bar{\mathbf{u}})]\nabla\zeta \\ &+ \frac{1}{2}\zeta(\nabla\cdot\bar{\mathbf{u}})^2\nabla h - \frac{1}{2}\zeta[\bar{\mathbf{u}}\cdot\nabla(\nabla\cdot\bar{\mathbf{u}})]\nabla h - \frac{1}{2}\zeta\nabla[\bar{\mathbf{u}}\cdot\nabla(\bar{\mathbf{u}}\cdot\nabla h)] - [\bar{\mathbf{u}}\cdot\nabla(\bar{\mathbf{u}}\cdot\nabla h)]\nabla\zeta,\end{aligned} \tag{43}$$

$$\mathbf{K_3} = \frac{2}{3}\zeta^2(\nabla\cdot\bar{\mathbf{u}})\nabla(\nabla\cdot\bar{\mathbf{u}}) - \frac{1}{3}\zeta^2\nabla[\bar{\mathbf{u}}\cdot\nabla(\nabla\cdot\bar{\mathbf{u}})] + \zeta(\nabla\cdot\bar{\mathbf{u}})^2\nabla\zeta - \zeta[\bar{\mathbf{u}}\cdot\nabla(\nabla\cdot\bar{\mathbf{u}})]\nabla\zeta. \tag{44}$$

Appendix B. Definition of the breaking terms

The breaking terms introduced in Eq. (20) are defined as follows:

$$\mathbf{\Delta M} = \begin{pmatrix} \Delta M_u & \Delta M_{uv} \\ \Delta M_{uv} & \Delta M_v \end{pmatrix}; \quad \mathbf{\Delta M_1} = \begin{pmatrix} \Delta M_{1u} & \Delta M_{1uv} \\ \Delta M_{1uv} & \Delta M_{1v} \end{pmatrix} \tag{45}$$

in which

$$\Delta M_u = \int_{-h}^{\delta\zeta}(u_r^2 - \bar{u}_r^2)dz, \tag{46}$$

$$\Delta M_{uv} = \int_{-h}^{\delta\zeta}(u_r v_r - \bar{u}_r\bar{v}_r)dz, \tag{47}$$

$$\Delta M_v = \int_{-h}^{\delta\zeta}(v_r^2 - \bar{v}_r^2)dz, \tag{48}$$

$$\Delta M_{1u} = -\frac{\partial}{\partial x}(\nabla\cdot\bar{\mathbf{u}}_\mathbf{p})\int_{-h}^{\delta\zeta}(2hz+z^2)(u_r-\bar{u}_r)dz, \tag{49}$$

$$\begin{aligned}\Delta M_{1uv} &= -\frac{1}{2}\int_{-h}^{\delta\zeta}(2hz+z^2)[(\mathbf{u_r}-\bar{\mathbf{u}}_\mathbf{r})\cdot\nabla^\star](\nabla\cdot\bar{\mathbf{u}}_\mathbf{p})dz = -\frac{1}{2}\frac{\partial}{\partial y}(\nabla\cdot\bar{\mathbf{u}}_\mathbf{p})\int_{-h}^{\delta\zeta}(2hz+z^2)(u_r-\bar{u}_r)dz \\ &\quad -\frac{1}{2}\frac{\partial}{\partial x}(\nabla\cdot\bar{\mathbf{u}}_\mathbf{p})\int_{-h}^{\delta\zeta}(2hz+z^2)(v_r-\bar{v}_r)dz,\end{aligned} \tag{50}$$

$$\Delta M_{1v} = -\frac{\partial}{\partial y}(\nabla\cdot\bar{\mathbf{u}}_\mathbf{p})\int_{-h}^{\delta\zeta}(2hz+z^2)(v_r-\bar{v}_r)dz, \tag{51}$$

$$\mathbf{\Delta P} = -\int_{-h}^{\delta\zeta}\int_{z}^{\delta\zeta}\int_{-h}^{z}(\mathbf{u_r}-\bar{\mathbf{u}}_\mathbf{r})dzdzdz, \tag{52}$$

$$\mathbf{D_w} = \int_{-h}^{\delta\zeta}\nabla\left\{\left[\nabla\cdot\int_{-h}^{z}(\mathbf{u_r}-\bar{\mathbf{u}}_\mathbf{r})dz\right]\left[\nabla\cdot\int_{-h}^{z}(2\bar{\mathbf{u}}+\mathbf{u_r}-\bar{\mathbf{u}}_\mathbf{r})dz\right]\right\}dz, \tag{53}$$

$$\begin{aligned}\mathbf{D_{sv}} &= \int_{-h}^{\delta\zeta}\nabla\left(\nabla\cdot\int_{z}^{\delta\zeta}v_t\frac{\partial\mathbf{u}}{\partial z}dz\right)dz \\ &= (h+\delta\zeta)\nabla[\nabla\cdot(v_t\mathbf{u_r}(\delta\zeta))] + \delta[\nabla\cdot(v_t\mathbf{u_r}(\delta\zeta))]\nabla\zeta \\ &\quad + \delta\nabla[v_t(\mathbf{u_r}(\delta\zeta)\cdot\nabla\zeta)] - \nabla\{\nabla\cdot[v_t(h+\delta\zeta)\bar{\mathbf{u}}_\mathbf{r}]\},\end{aligned} \tag{54}$$

$$\begin{aligned}\mathbf{D_{sh}} &= \nabla^\star\int_{-h}^{\delta\zeta}v_t(\nabla^\star\cdot\mathbf{u})dz \\ &= (h+\delta\zeta)\nabla^\star[v_t(\nabla^\star\cdot\bar{\mathbf{u}})] + \delta v_t(\nabla^\star\cdot\bar{\mathbf{u}})\nabla^\star\zeta \\ &\quad - \delta\nabla^\star[v_t(\mathbf{u_r}(\delta\zeta)\cdot\nabla^\star\zeta)] + \delta\nabla^\star[v_t(\bar{\mathbf{u}}_\mathbf{r}\cdot\nabla^\star\zeta)],\end{aligned} \tag{55}$$

$$\mathbf{D_{uw}} = \int_{-h}^{\delta\zeta}\nabla\left\{\nabla\cdot\int_{z}^{\delta\zeta}\left[(\mathbf{u_r}-\bar{\mathbf{u}}_\mathbf{r})\nabla\cdot\int_{-h}^{z}\bar{\mathbf{u}}dz + (\bar{\mathbf{u}}+\mathbf{u_r}-\bar{\mathbf{u}}_\mathbf{r})\nabla\cdot\int_{-h}^{z}(\mathbf{u_r}-\bar{\mathbf{u}}_\mathbf{r})dz\right]dz\right\}dz. \tag{56}$$

Appendix C. Calculation of the breaking terms

The vorticity transport equation is expressed and solved analytically along the direction of propagation of the waves. It is necessary to express the breaking terms with respect to the generic subgrid abscissa s. In such a way the two vectorial components of these variables can be mutated into one, and the variables become scalars.

Therefore, the ∇ operator can be substituted with the simple partial derivative $\partial/\partial s$. This passage from the modulus of the gradient to the partial derivative along the direction of wave propagation is better specified. In particular, considering that the scheme in Fig. 2 is valid for the generic function F, the absolute value of the partial derivative of F becomes:

$$\left|\frac{\partial F}{\partial s}\right| = \left|\cos\alpha\frac{\partial F}{\partial x} + \sin\alpha\frac{\partial F}{\partial y}\right|. \tag{57}$$

Moreover, it is possible to write the modulus of the gradient of F as the sum of the projection of its components along x and y directions

$$|\nabla F| = \left|\cos\beta\frac{\partial F}{\partial x} + \sin\beta\frac{\partial F}{\partial y}\right|. \tag{58}$$

Following such a derivation, the modulus of the gradient of the generic function F coincides with the absolute value of the partial derivative along the wave propagation s only when $\beta = \alpha$, namely, when the direction in which the gradient of F is located is the same as s. Therefore, if the breaking terms follows the behavior of the waves, i.e. if such terms have the greatest spatial variation along the direction of propagation of the waves, the hypothesis of substituting gradients with partial derivative along s is reasonable and therefore:

$$|\nabla F| = \left|\frac{\partial F}{\partial s}\right|. \tag{59}$$

In conclusion the breaking terms in the momentum equation, i.e. $\nabla(\boldsymbol{\Delta M})$, $\nabla(\boldsymbol{\Delta M_1})$, $[\nabla(\nabla\cdot\boldsymbol{\Delta P})]_t$, $\mathbf{D_w}$, $(\mathbf{D_{sv}}+\mathbf{D_{sh}})$ and $\mathbf{D_{uw}}$, can be redefined in scalar form as follows

$$\frac{\partial \Delta M}{\partial s};\quad \frac{\partial \Delta M_1}{\partial s};\quad \left(\frac{\partial^2 \Delta P}{\partial s^2}\right)_t;\quad D_w;\quad D_s;\quad D_{uw}. \tag{60}$$

Although the hypothesis that α is equal to β mentioned in Section 2 for the velocity vector, the extension to other variables, the breaking terms, deserves some attention. For example, the planar distribution of the breaking terms was analysed for the submerged shoal case. In particular, Fig. 15 shows the spatial distribution of ΔM along a wave period in the area where the vorticity was analysed in Section 5. It can be observed that the rate of spatial variation of one of the leading order breaking terms along the streamwise direction is at least double with respect to the same variation in the spanwise direction.

Moreover, the terms correlated with the eddy viscosity (namely $\mathbf{D_{sv}}$ and $\mathbf{D_{sh}}$) were reduced to one, i.e. D_s, correlated with the turbulence in the vertical plane. This can be justified since turbulence in the vertical direction is expected to be more important in the area near the roller region.

Since the breaking terms expressed in scalar form act on the s axis, it is possible to obtain the terms starting from their projection in that direction:

$$(\Delta M)_s = \frac{\partial}{\partial s}\int_h^{\delta\zeta}(u_r^2 - \overline{u}^2)dz, \tag{61}$$

$$(\Delta M_1)_s = \frac{\partial}{\partial s}\left[-\overline{u}_{pss}\int_{-h}^{\delta\zeta}(2hz+z^2)(u_r-\overline{u}_r)dz + O(h_s)\right], \tag{62}$$

$$\Delta P = -\int_{-h}^{\delta\zeta}\int_z^{\delta\zeta}\int_{-h}^{z}(u_r-\overline{u}_r)dzdzdz, \tag{63}$$

$$D_w = \int_{-h}^{\delta\zeta}\frac{\partial}{\partial s}\left[\left(\frac{\partial}{\partial s}\int_{-h}^{z}(u_r-\overline{u}_r)dz\right)\left(\frac{\partial}{\partial s}\int_{-h}^{z}(2\overline{u}+u_r-\overline{u}_r)dz\right)\right]dz, \tag{64}$$

$$D_s = (h+\delta\zeta)[\nu_t u_r(\delta\zeta)]_{ss} + \delta\zeta_s[\nu_t u_r(\delta\zeta)]_s + \delta[\nu_t u_r(\delta\zeta)\zeta_s]_s - [\nu_t\overline{u}_r(h+\delta\zeta)]_{ss}, \tag{65}$$

$$D_{uw} = \int_{-h}^{\delta\zeta}\frac{\partial^2}{\partial s^2}\int_z^{\delta\zeta}\left[(u_r-\overline{u}_r)\frac{\partial}{\partial s}\int_{-h}^{z}\overline{u}dz + (\overline{u}+u_r-\overline{u}_r)\frac{\partial}{\partial s}\int_{-h}^{z}(u_r-\overline{u}_r)dz\right]dzdz. \tag{66}$$

In the equations the subscript $(_s)$ represent the partial derivative in this direction. Moreover, all the velocities are related to the same axis. In particular, the rotational velocity u_r can be derived from the two-dimensional formulation obtained in Eq. (17), by a simple projection along s

$$u_r = \int_{-h}^{z}\omega dz + O(\mu^2), \tag{67}$$

where the dispersive terms $O(\mu^2)$ are neglected in all the breaking terms in which u_r appears, since it has to be multiplied for other terms of the same order, thus becoming the order of $O(\mu^4)$ and then negligible.

The derivation of the previous breaking terms of the proposed model starts from the definition of rotational velocity, and consequently the distribution of vorticity along the water column, which, following the definition of the region for integration of the vorticity transport equation, can be expressed as

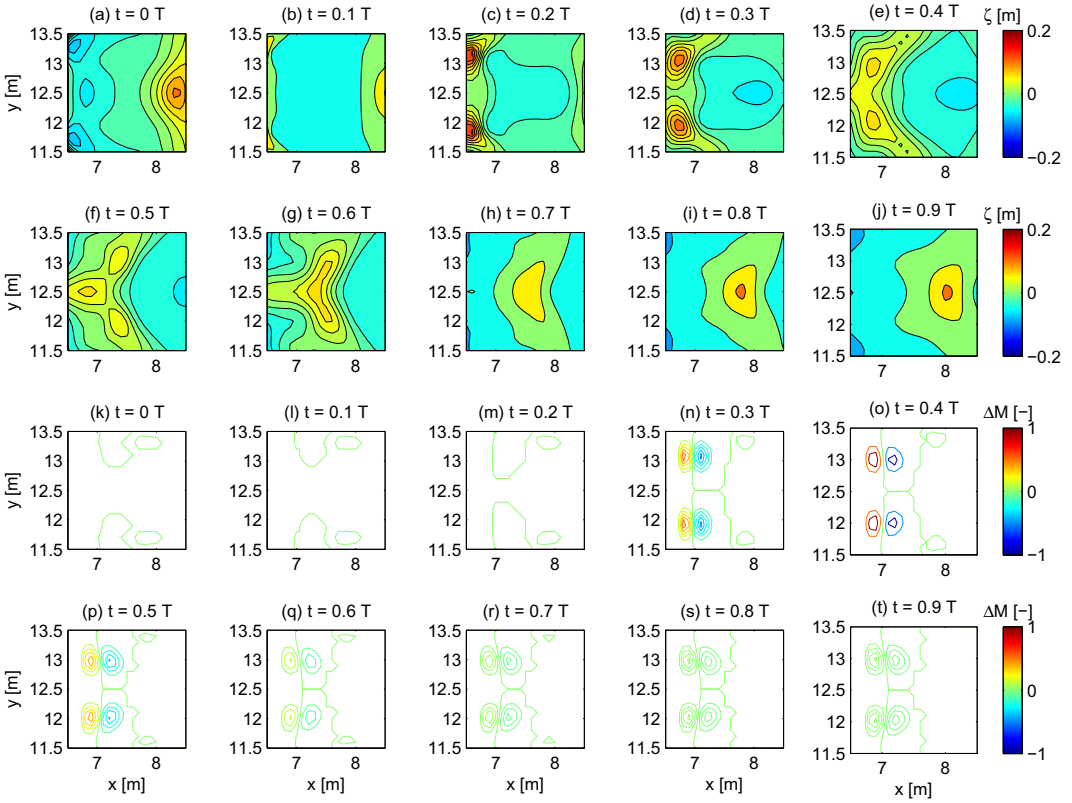

Fig. 15. Free surface elevations (a)–(j) and ΔM (k)–(t) at ten instants within a wave period.

$$\omega = \begin{cases} \sum_{n=1}^{\infty} G_n \sin n\pi\sigma & z < \zeta_e, \\ \omega_s\left(\frac{\zeta - z}{\zeta - \zeta_e}\right) & \zeta_e < z < \zeta. \end{cases} \tag{68}$$

In such way the rotational velocity should be written as:

$$u_r = \begin{cases} u_r = \int_{-h}^{z} \omega dz & z < \zeta_e, \\ u_{rb} + \int_{\zeta_e}^{z} \omega dz & \zeta_e < z < \zeta, \end{cases} \tag{69}$$

where u_{rb} is the rotational velocity at the lower edge of the roller.

As reported in Musumeci et al. [22], the expressions used for computing the breaking terms were derived assuming that for the $O(\mu^2)$ terms, namely ΔP_{sst}, D_{uw}, ΔM_1 and D_w, the contribution coming from the roller region was assumed to be small. Thus, substituting the expression for rotational velocity in Eqs. (61)–(66), having applied algebra, the breaking terms read:

$$\begin{aligned} \Delta M \; &= (h+\zeta_e)^3 \left[\left(\sum_{n=1}^{\infty} \frac{G_n}{n\pi} \right)^2 + \frac{1}{2} \sum_{n=1}^{\infty} \frac{G_n^2}{n^2\pi^2} \right] + u_{rb}^2 (\zeta - \zeta_e) + \frac{2}{3} u_{rb} \omega_s (\zeta - \zeta_e)^2 + \frac{2}{15} \omega_s^2 (\zeta - \zeta_e)^3 \\ &- \frac{\left[(h+\zeta_e)^2 \sum_{n=1}^{\infty} \frac{G_n}{n\pi} + u_{rb}(\zeta - \zeta_e) + \frac{1}{3}\omega_s (\zeta - \zeta_e) \right]}{h+\zeta} \end{aligned} \tag{70}$$

$$(\Delta P)_{sst} = \frac{\partial^2}{\partial s^2} \left(-(h+\zeta_e)^4 \sum_{n=1}^{\infty} \frac{\partial G_n}{\partial t} \frac{(-1)^n}{n^3\pi^3} - 4(h+\zeta_e)^3 \frac{\partial \zeta_e}{\partial t} \sum_{n=1}^{\infty} \frac{G_n (-1)^n}{n^3\pi^3} \right) \tag{71}$$

$$D_{uw} = \frac{\partial^2}{\partial s^2}\left[(h+\zeta_e)^4 + \frac{\partial \overline{u}}{\partial s}\sum_{n=1}^{\infty}\frac{G_n}{n^3\pi^3}(-1)^n + 2(h+\zeta_e)^3\overline{u}\frac{\partial \zeta_e}{\partial s}\sum_{n=1}^{\infty}\frac{G_n}{n^3\pi^3}(-1)^n + (h+\zeta_e)^4\overline{u}\sum_{n=1}^{\infty}\frac{\partial G_n}{\partial s}\frac{(-1)^n}{n^3\pi^3}\right.$$
$$+ (h+\zeta_e)^3\overline{u}\frac{\partial \zeta_e}{\partial s}\sum_{n=1}^{\infty}\left(1+(-1)^n\right) + \frac{1}{2}(h+\zeta_e)^4\frac{\partial \zeta_e}{\partial s}\sum_{n=1}^{\infty}\frac{G_n^2}{n^4\pi^4} - 2(h+\zeta_e)^4\frac{\partial \zeta_e}{\partial s}\sum_{n=1}^{\infty}\sum_{\substack{m=1\\m\neq n}}^{\infty}\frac{G_nG_m}{nm\pi^4(n^2-m^2)}$$
$$+ \frac{1}{4}(h+\zeta_e)^5\sum_{n=1}^{\infty}\frac{G_n}{n^4\pi^4}\frac{\partial G_n}{\partial s} - (h+\zeta_e)^5\sum_{n=1}^{\infty}\sum_{\substack{m=1\\m\neq n}}^{\infty}\frac{G_n}{nm\pi^4}\frac{\partial G_m}{\partial s}\frac{1}{n^2-m^2} - (h+\zeta_e)^4\frac{\partial \zeta_e}{\partial s}\sum_{n=1}^{\infty}\frac{G_n^2}{n^2\pi^2}\left(\frac{1}{12}-\frac{1}{4n^2\pi^2}\right)$$
$$\left.+(h+\zeta_e)^4\frac{\partial \zeta_e}{\partial s}\sum_{n=1}^{\infty}\sum_{\substack{m=1\\m\neq n}}^{\infty}\frac{G_nG_m}{nm\pi^4}\frac{(-1)^{n+m}}{(n+m)^2}\right], \tag{72}$$

$$\Delta M_1 = 2\overline{u}_{pss}(h+\zeta_e)^4\sum_{n=1}^{\infty}\frac{G_n}{n^3\pi^3}(-1)^n, \tag{73}$$

$$D_w = \frac{\partial}{\partial s}\left[8\frac{\partial \overline{u}}{\partial s}\frac{\partial \zeta_e}{\partial s}(h+\zeta_e)^3\sum_{n=1}^{\infty}\frac{G_n}{n^3\pi^3}(-1)^n + 2\frac{\partial \overline{u}}{\partial s}(h+\zeta_e)^4\sum_{n=1}^{\infty}\frac{\partial G_n}{\partial s}\frac{(-1)^n}{n^2\pi^2} + \frac{13}{4}(h+\zeta_e)^3\left(\frac{\partial \zeta_e}{\partial s}\right)^2\sum_{n=1}^{\infty}\frac{G_n^2}{n^4\pi^4}\right.$$
$$+ \frac{1}{2}(h+\zeta_e)^5\sum_{n=1}^{\infty}\frac{1}{n^4\pi^4}\left(\frac{\partial G_n}{\partial s}\right)^2 + \frac{1}{6}(h+\zeta_e)^3\left(\frac{\partial \zeta_e}{\partial s}\right)^2\sum_{n=1}^{\infty}\sum_{\substack{m=1\\m\neq n}}^{\infty}\frac{G_nG_m}{nm\pi^4}\times\frac{2(n^2+m^2)+4(n^2-m^2)\pi^2}{(n^2-m^2)\pi^2}$$
$$\left.+\frac{5}{2}(h+\zeta_e)^4\frac{\partial \zeta_e}{\partial s}\sum_{n=1}^{\infty}\frac{G_n}{n^4\pi^4}\frac{\partial G_n}{\partial s} + 2(h+\zeta_e)^4\frac{\partial \zeta_e}{\partial s}\sum_{n=1}^{\infty}\sum_{\substack{m=1\\m\neq n}}^{\infty}\frac{\partial G_n}{\partial s}\frac{G_m}{nm\pi^4}\frac{(-1)^{n+m}}{n^2-m^2}\right]. \tag{74}$$

References

[1] P.A. Madsen, R. Murray, O.R. Sørensen, A new form of the Boussinesq equations with improved linear dispersion characteristics, Coastal Eng. 15 (1991) 371–388.
[2] G. Wei, J.T. Kirby, S.T. Grilli, R. Subramanya, A fully non linear Boussinesq model for surface waves. I: Highly non linear, unsteady waves, J. Fluid Mech. 294 (1995) 71–92.
[3] S. Beji, K. Nadaoka, A formal derivation and numerical modelling of the improved Boussinesq equations for varying depth, Ocean Eng. 23 (1996) 691–704.
[4] P.A. Madsen, H.A. Schäffer, Higher-order Boussinesq-type equations for surface gravity waves: derivation and analysis, Philos. Trans. R. Soc. London A 356 (1998) 3123–3184.
[5] M.F. Gobbi, J.T. Kirby, Wave evolution over submerged sills: tests of a high order Boussinesq model, Coastal Eng. 37 (1999) 57–96.
[6] P.A. Madsen, H.B. Bingham, H.A. Schäffer, Boussinesq-type formulations for fully nonlinear and extremely dispersive water waves: derivation and analysis, Proc. R. Soc. London A 459 (2003) 1075–1104.
[7] P. Lynett, P.L.F. Liu, A two-layer approach to wave modelling, Proc. R. Soc. London A 460 (2004) 2637–2669.
[8] P.A. Madsen, D.R. Fuhrman, B. Wang, A Boussinesq-type method for fully nonlinear waves interacting with a rapidly varying bathymetry, Coastal Eng. 53 (2006) 487–504.
[9] H.B. Bingham, P.A. Madsen, D.R. Fuhrman, Velocity potential formulations of highly accurate Boussinesq-type models, Coastal Eng. 56 (2009) 467–478.
[10] P. Lin, C. Man, A staggered-grid numerical algorithm for the extended Boussinesq equations, Appl. Math. Model. 31 (2007) 349–368.
[11] Y.S. Li, S.X. Liu, Y.X. Yu, G.Z. Lai, Numerical modelling of multi-directional irregular waves through breakwaters, Appl. Math. Model. 24 (2000) 551–574.
[12] S.X. Liu, B. Teng, Y.X. Yu, Wave generation in a computation domain, Appl. Math. Model. 31 (2005) 349–368.
[13] S.X. Liu, Z. Sun, J. Li, An unstructured FEM model based on Boussinesq equations and its application to the calculation of multidirectional wave run-up in a cylinder group, Appl. Math. Model. 6 (2012) 4146–4164.
[14] A.B. Kennedy, Q. Chen, J.T. Kirby, R.A. Dalrymple, Boussinesq modeling of wave transformation, breaking and run-up. I: 1D, J. Waterway Port Coastal Ocean Eng. 126 (2000) 39–47.
[15] H.A. Schäffer, P.A. Madsen, R. Deigaard, A Boussinesq model for waves breaking in shallow water, Coastal Eng. 20 (1993) 185–202.
[16] F. D'Alessandro, G.R. Tomasicchio, The BCI criterion for the initiation of breaking process in Boussinesq-type equations wave models, Coastal Eng. 55 (2008) 1174–1184.
[17] J.A. Zelt, The run-up of nonbreaking and breaking solitary waves, Coastal Eng. 15 (1991) 205–246.
[18] P.A. Madsen, O.R. Sørensen, H.A. Schäffer, Surf zone dynamics simulated by a Boussinesq type model. Part I: Model description and cross-shore motion of regular waves, Coastal Eng. 32 (1997) 255–287.
[19] J. Veeramony, I.A. Svendsen, The flow in the surf-zone waves, Coastal Eng. 39 (2000) 93–122.
[20] T.V. Karambas, N.P. Tozer, Breaking waves in the surf and swash zone, J. Coastal Res. 19 (2003) 514–528.
[21] R. Briganti, R.E. Musumeci, G. Bellotti, M. Brocchini, E. Foti, Boussinesq modeling of breaking waves: description of turbulence, J. Geophys. Res. 109 (2004).
[22] R.E. Musumeci, I.A. Svendsen, J. Veeramony, The flow in the surf zone: a fully nonlinear Boussinesq-type of approach, Coastal Eng. 52 (2005) 565–598.
[23] Q. Chen, J.T. Kirby, R.A. Dalrymple, A.B. Kennedy, A. Chawla, Boussinesq modeling of wave transformation, breaking and run-up. I: 2D, J. Waterway Port Coastal Ocean Eng. 126 (2000) 48–56.
[24] I.A. Svendsen, Wave heights and set-up in a surf zone, Coastal Eng. 8 (1984) 303–329.
[25] K. Nadaoka, M. Hino, Y. Koyano, Structure of the turbulent flow field under breaking waves in the surf zone, J. Fluid Mech. 204 (1989) 359–387.
[26] D.T. Cox, N. Kobayashi, A. Okaiasucox, Experimental and numerical modeling of surf zone hydrodynamics, Research report CACR-95-07, Center For Applied Coastal Research, University of Delaware, 1995.
[27] P. Madsen, H.A. Schäffer, A review of Boussinesq-type equations for gravity waves, in: P.L.-F. Liu (Ed.), Advances in Coastal and Ocean Engineering, vol. 5, World Scientific, Singapore, 1998.
[28] Y. Watanabe, H. Saeki, R.J. Hosking, Three-dimensional vortex structures under breaking waves, J. Fluid Mech. 545 (2005) 291–328.
[29] F.C.K. Ting, Large-scale turbulence under a solitary wave. Part 2: Forms and evolution of coherent structures, Coastal Eng. 55 (2008) 522–536.

[30] F.C.K. Ting, J.R. Nelson, Laboratory measurements of large-scale near-bed turbulent flow structures under spilling regular waves, Coastal Eng. 58 (2011) 151–172.
[31] J. Battjest, Computation of set-up, longshore currents, run-up and overtopping due to wind generated waves (Ph.D. thesis), 1974.
[32] A.R. van Dongeren, I.A. Svendsen, Absorbing-generating boundary condition for shallow water models, J. Waterway Port Coast Ocean Eng. 123 (1997) 303–313.
[33] I.A. Svendsen, J. Veeramony, J. Bakunin, J. Kirby, The flow in weak turbulent hydraulic jump, J. Fluid Mech. 418 (2000) 25–57.
[34] O.R. Sørensen, H.A. Schäffer, P.A. Madsen, Surf zone dynamics simulated by a Boussinesq type model. Part III: Wave induced horizontal nearshore circulations, Coastal Eng. 32 (1998) 255–287.
[35] O.R. Sørensen, H.A. Schäffer, L.S. Sørensen, Boussinesq-type modelling using an unstructured finite element technique, Coastal Eng. 50 (2004) 181–198.
[36] J.B. Hansen, I.A. Svendsen, Regular waves in shoaling water experimental data, Series Paper 21, Institute of Hydrodynamics and Hydraulic Engineering, Technical University of Denmark, 1979.
[37] Z.C. Huang, S.C. Hsiao, H.H. Hwung, K.A. Chang, Turbulence and energy dissipations of surf-zone spilling breakers, Coastal Eng. 56 (2009) 733–746.
[38] A.S. Dimakopoulos, A.A. Dimas, Large-wave simulation of three-dimensional, cross-shore and oblique, spilling breaking on constant slope beach, Coastal Eng. 58 (2011) 790–801.
[39] C.L. Vincent, M.J. Briggs, Refraction–diffraction of irregular waves over a mound, J. Waterway Port Coast Ocean Eng. 115 (1989) 269–284.